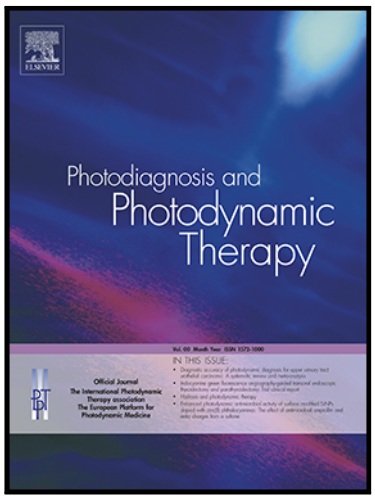

Ionizing radiation and photodynamic therapy led to multimodal tumor cell death, synergistic cytotoxicity and immune cell invasion in human bladder cancer organoids

Annabell Reinhold , Annegret Glasow , Sandra Nürnberger , Annett Weimann , Lucie Telemann , Jens-Uwe Stolzenburg , Jochen Neuhaus , Mandy Berndt-Paetz

PII: S1572-1000(24)00495-2
DOI: https://doi.org/10.1016/j.pdpdt.2024.104459
Reference: PDPDT 104459

To appear in: *Photodiagnosis and Photodynamic Therapy*

Received date: 9 October 2024
Revised date: 20 December 2024
Accepted date: 26 December 2024

Please cite this article as: Annabell Reinhold , Annegret Glasow , Sandra Nürnberger , Annett Weimann , Lucie Telemann , Jens-Uwe Stolzenburg , Jochen Neuhaus , Mandy Berndt-Paetz , Ionizing radiation and photodynamic therapy led to multimodal tumor cell death, synergistic cytotoxicity and immune cell invasion in human bladder cancer organoids, *Photodiagnosis and Photodynamic Therapy* (2024), doi: https://doi.org/10.1016/j.pdpdt.2024.104459

HIGHLIGHTS

- Combinational therapy of PDT and ionizing radiation in bladder-like organoids presented
- IR and PDT using the near-infrared photosensitizer THPTS resulted in highly tumor-selective, synergistic cytotoxicity.
- IR+PDT provoked multimodal cell death involving apoptosis, necroptosis, ferroptosis and/or pyroptosis
- IR+PDT led to recruitment of immune cells

Titel: Ionizing radiation and photodynamic therapy led to multimodal tumor cell death, synergistic cytotoxicity and immune cell invasion in human bladder cancer organoids

Authors:

Annabell Reinhold[1], Annegret Glasow[2], Sandra Nürnberger[1], Annett Weimann[1], Lucie Telemann[3], Jens-Uwe Stolzenburg[3], Jochen Neuhaus[1], Mandy Berndt-Paetz[1#]

Affiliations:

[1] Dept. of Urology, Research Laboratories, University of Leipzig, Liebigstraße 19, 04103 Leipzig, Germany;

[2] Dept. of Radiation Therapy, University of Leipzig, Stephanstraße 9a, 04103 Leipzig, Germany;

[3] Dept. of Urology, University Hospital Leipzig, Liebigstraße 20, 04103 Leipzig, Germany

 # Correspondence:

Mandy Berndt-Paetz

Dept. of Urology, Research Laboratories, University of Leipzig

Liebigstraße 19, Building C, 04103 Leipzig (Germany)

Tel.: +49 341 9717654, Fax: +49 341 9717659

Email: mandy.berndt@medizin.uni-leipzig.de

Wordcount: 4412 words; **Figures:** 4; **Tables:** 1; **Supplements:** 7

ABSTRACT

Background: Photodynamic therapy (PDT) and radiotherapy using ionizing radiation (IR) are promising options for organ-preserving treatment of bladder cancer (BCa). A combination therapy (IR+PDT) could be beneficial for BCa treatment.

Purpose: For PDT, we used the near-infrared photosensitizer tetrahydroporphyrin-tetratosylate (THPTS) showing high therapeutic efficacy. Treatment responses were analyzed in BCa organoids.

Methods: Organoids consisting of BCa cells lines, bladder fibroblasts and muscle cells were treated with IR (9 Gy) and/or PDT using THPTS (25, 50 µM; 20 J/cm^2). Cytotoxicity was determined by microscopy, cell-based assays and histology. The cell death mode was

analyzed by applying specific inhibitors followed by immunofluorescence or qPCR analyses of cell death markers. A matrix-based co-culture model was used to study T cell migration into the environment of treated organoids.

Results: PDT and/or IR resulted in concentration-dependent reduction of metabolic activity, organoid diameter and integrity. Higher cytotoxicity of IR+PDT vs. monotherapies was observed after 72 h. Non-malignant organoids showed no cytotoxic effects. While apoptosis, necroptosis and ferroptosis were clearly involved in cell death of T-24 cells, cytotoxicity in RT-112 cells was probably provoked by apoptosis, ferroptosis and pyroptosis. IR+PDT resulted in significant migration of Jurkat cells into ECM-embedded organoids within 3 days after treatment.

Conclusion: Treatment with IR+PDT showed tumor-selective cytotoxicity with additive or synergistic effects in BCa organoids. Thereby, IR+PDT led to multimodal cell death depending on the cellular context. Migration of T cells into the organoid environment illustrates the immunogenic potential of IR+PDT. Therefore, it might be a promising approach for organ-preserving BCa treatment.

KEYWORDS

Photodynamic therapy; near-infrared photosensitizer; ionizing radiation; bladder cancer organoids; multimodal, synergistic cytotoxicity; immune cell invasion

INTRODUCTION

Bladder cancer (BCa) is the 10th most common cancer worldwide [1]. At initial diagnosis, 75% of the patients have a non-muscle-invasive BCa, while 25% already have a muscle-invasive disease. Standard treatment for non-muscle-invasive BCa is transurethral resection and intravesical chemotherapy. In spite of this therapy, approximately 43% of non-muscle-invasive BCa will relapse and about 8% will progress to muscle-invasive disease [2]. In high-grade non-muscle-invasive and in muscle-invasive BCa, bladder removal with postoperative adjuvant chemotherapy is recommended. To date, there are no generally accepted options of organ preserving therapies [3]. Radical surgery is always associated with significant quality of life limitations. In addition, resistance of tumor cell populations to chemotherapy causes tumor progression or tumor relapse [4]. Thus, development of new bladder-sparing treatment methods is an important translational avenue in urological research. Approval of immunotherapy with antibodies to PD-1 / PD-L1 is a major, recent advance in cancer therapy. However, treatment with PD-L1 inhibitors is only applicable in patients with high PD-L1

expression [5,6]. This further demonstrates the need for other effective, gentle treatment options. Focal therapies such as photodynamic therapy (PDT) and radiotherapy are promising options for minimal-invasive treatment of urothelial cancer. These methods exclusively target the tumor-bearing tissue areas, whereas adjacent, healthy tissue is largely spared and the systemic burden is low [7–9].

PDT is based on photoactivation of a non-toxic light reactive agent, so-called photosensitizer (PS), by a specific wavelength in presence of tissue oxygen. PSs preferentially accumulate in cancer cells and localize mainly to mitochondria or lysosomes. Activation leads to the production of reactive oxygen species (ROS) and singlet oxygen ($^1O_2$) which results in direct tumor cell death [10]. Radiotherapy using IR induces direct damages to the DNA causing single- and double-strand breaks. Subsequently, IR generates free radicals and ROS which results in a mixture of cellular events [11]. PDT and radiotherapy can cause cancer cell death via a combination of various cell death modes, e.g. apoptosis, necroptosis, pyroptosis, ferroptosis and necrosis [12,13]. Damage-associated molecular patterns (DAMPs) are released or surface-exposed by cancer cells following so-called immunogenic cell death, which could prime the immune system for further destruction of persistent primary tumor cells, concurrent metastatic disease and may also reduce tumor recurrence [12–16].

In previous studies, we characterized the effects of the near-infrared photosensitizer tetrahydroporphyrin-tetratosylate (THPTS) intended for PDT of BCa. The water-soluble and positively charged THPTS has an absorption maximum at 760.5 nm, thus allowing up to 15 mm tissue penetration [17–19]. This enables treatment of larger solid tumors and may even permit the treatment of muscle-invasive BCa. Local THPTS-PDT resulted in significant reduction of muscle-invasive tumors and showed no photodynamic side effects in an orthotopic rat bladder cancer model [18]. THPTS localized mainly to lysosomes of BCa cells and led to production of intracellular ROS after laser irradiation [17]. Radiotherapy causes damage to the DNA in the nucleus of tumor cells [15,20]. It is well-documented that combinations of differentially acting therapies can siginificantly enhance the tumoricidal and immunogenic effects [12]. The use of PDT with THPTS in combination with ionizing radiation (IR) was already shown to be a promising approach for treatment of human glioblastoma cells. In this study, the combinational therapy led to synergistic cytotoxicity in vitro and in vivo [21]. Here, we present the cellular effects of THPTS-PDT in combination with IR in our recently established BCa organoid model, which showed an inverse bladder-like structure with a peripheral cytokeratin-positive BCa layer [22]. We characterize concentration- and cell line-dependent cytotoxicity as well as induced cell death pathways. Futhermore, we investigated the immunogenic effects in a matrix-based co-culture model with T cells.

MATERIAL AND METHODS

Cell culture

Five human BCa cell lines of various origin (Supplementary Table S1) were obtained from the Leibniz Institute DSMZ (German collection of microorganisms and cell cultures GmbH, Braunschweig, Germany): RT-4 (RRID:CVCL_0036), RT-112 (RRID:CVCL_1670), KU-19-19 (RRID:CVCL_1344), T-24 (RRID:CVCL_0554), CAL-29 (RRID:CVCL_1808).

Spontaneously immortalized human bladder epithelial progenitors (HBLAK) were obtained from CELLnTEC and were grown in CnT-Prime Epithelial Culture Medium (Cat.-No.: CnT-PR; CELLnTEC, Bern, Switzerland). Primary human bladder fibroblasts (hBF, Cat.-No.: FC-0050) and human bladder smooth muscle cells (hBSMC, Cat.-No.: FC-0043) were both purchased from CellSystems (Troisdorf, Germany). The human T cell leukemia cell line Jurkat (RRID:CVCL_0065) was obtained from the DSMZ (German collection of microorganisms and cell cultures GmbH, Braunschweig, Germany). All BCa cells and Jurkat cells were cultured in RPMI1640 medium supplemented with 10% FBS (Biochrom, Berlin, Germany) and 1% CTS™ GlutaMAX™-I Supplement (Cat.-No.: A1286001; Thermo Fisher Scientific, Dreieich, Germany). The hBF were cultured in FibroLife® S2 medium (Cat.-No.: LL-0011) and hBSMC were cultured in VascuLife® SMC medium (Cat.-No.: LL-0014; Lifeline Cell Technology, Frederick, USA). Cells were maintained at 37°C and 5% CO2 in humidified atmosphere. To obtain single-cell suspension of each adherent cell line, Accutase cell detachment solution (Cat.-No.: P10-21500; PanBiotech, Aidenbach, Germany) was applied.

Generation of standardized BCa organoids

The ultra-low attachment (ULA) microplate method was used for organoid formation. To generate BCa organoids, BCa cells were mixed with hBF and hBSMC at equal quantities (4.000 cells each). For hBF/hBSMC organoid construction, hBF and hBSMC (6.000 cells each) were mixed. The cell suspensions (12.000 cells per well) were centrifuged (250 x g; 5 min) into Corning® Spheroid microplates (black; Cat.-No.: 4520; Corning Inc., Kennebunk, USA). BCa and hBF/hBSMC organoids were cultured in a 1:1:1 mixture of cell type-specific media for 3 days until IR and/or PDT treatment. HBLAK organoids were constructed by co-culturing of HBLAK, hBF, hBSMC (4.000 cells each) for 14 days in 1:1:1 mixture of cell type-specific media, including differentiation medium for the HBLAK cells (CnT-Prime Epithelial 2D Differentiation Medium, Cat.-No.: CnT-PR-D, CELLnTEC, Bern, Switzerland; 1.2 mM Ca).

Ionizing radiation and PDT

Samples were treated by IR 1 h before PS incubation using an orthovoltage X-ray machine (Xstrahl 200, Xstrahl, Ratingen, Germany). Irradiation was applied as single dose (9 Gy) at a dose rate of 1.43 Gy/min (150 kV, 10 mA). Sham irradiated controls were shielded by MCP-96 blocks. THPTS ($C_{72}H_{70}N_8O_{12}S_4$; MW: 1767.66 Da, purity ≥ 95%) was otained from TetraPDT GmbH (Leipzig, Germany). Samples were then treated with 25, 50 µM THPTS (diluted in organoid culture medium) freshly prepared from a 10 mM water stock solution. After 120 minutes of incubation, medium was replaced and organoids were irradiated at 760 nm using a diode laser (3W, 760 ± 5 nm, LAMI-Helios, TetraPDT GmbH, Rackwitz, Germany). Laser light was delivered via a glass fibre coupled to the laser producing a beam spot of 2 cm. Laser light intensity was measured and adjusted using a laser power meter (LaserStar, Ophir Optronics, Darmstadt, Germany). A light dose of 20 J/cm^2 was delivered at an intensity of 0.8 W/cm^2 for 20 seconds (at a 4 cm light-to-sample distance). The wells were irradiated individually; the other samples were protected from laser light with a cover plate. After PDT, organoids were incubated for indicated time periods and assayed for cytotoxic effects.

Treatment response

After treatment, organoids were cultured for additional 24, 48, 72 and 96 h. Images of organoids were acquired at indicated time periods using a Keyence BZ-X800 microscope (Keyence Coorporation, Osaka, Japan). Organoid sizes were measured by finding the maximum organoid diameter using the Keyence BZ-X800 Analyzer software. For analyzing the loss of morphological integrity, optical density was measured by selecting organoids as region of interest (ROI) in Fiji, including ImageJ version 1.53 (RRID: SCR_003070) [23]. A calibrated optical density 8-bit step tablet was used to calibrate the image. Metabolic activity was determined using the CellTiter-Glo® 3D Cell Viability Assay (Cat.-No.: G9681; Promega, Mannheim, Germany) measured on a microplate reader (SpectraMax M5, Molecular Devices, Sunnyvale, USA).

Inhibitors

Specific inhibitors against apoptosis (25 µM Z-VAD-FMK; Cat.-No.: FMK001, R&D Systems, Minneapolis, MN, USA), ferroptosis (0.5 µM ferrostatin-1 (Cat.-No.: SML0583; 25 µM deferoxamine mesylate (DFO, Cat.-No.: D9533), Sigma-Aldrich, Munich, Germany) and necroptosis (25 µM necrostatin-1 (Cat.-No.: 480065); 25 µM GSK`872 (Cat-No.: 5.30389); 25 µM MLKL-i (Cat.-No.: 480073); Sigma-Aldrich, Munich, Germany) were applied during medium exchange after THPTS incubation. Inhibitory effects were determined using the CellTiter-Glo® 3D Cell Viability Assay.

Cell invasion assay

Organoids were embedded into ECM (mixed with culture medium; ratio 1:1) directly after treatment with IR+PDT (9 Gy; 50 µM THPTS; light dose 20 J/cm^2) or 2 µM mitoxantrone (ICD-inducer; [24]). Mitoxantrone (Cat.-No.: M6545) and ECM gel (Cat.-No.: E1270) were purchased from Sigma-Aldrich (Munich, Germany). Organoid-bearing ECM layers were co-cultured with culture medium supernatants containing Jurkat cells (10.000 cells per well). Total Jurkat cell numbers in supernatants were counted after 3 days. Invasion of Jurkats into organoid environment was further verified by anti-CD3 staining (DAB) of histologically processed organoid samples.

Histology and DAB immunostaining

Organoids were fixed by 4% paraformaldehyde and embedded into HistoGel (Cat.-No.: FIS12608606; ThermoFisher Scientific, Dreieich, Germany) 72 h after treatment. Serial sections at 4 µm were HE-stained and immunostained following paraffin embedding. For DAB staining, sections were deparaffinized followed by antigen retrieval using heat-induced epitope retrieval buffer, pH 9.0 (Cat.-No.: ZUC029; Zytomed Systems, Berlin, Germany) for 40 minutes at 100°C. After blocking of endogenous peroxidase, sections were treated with primary antibodies (Table 1) overnight at 4°C. Biotin-linked goat-anti-mouse secondary antibody (Cat.-No.: BA-9200-1.5; Vector Laboratories, Newark, USA) was incubated 45 minutes at room temperature. Following a coupling step with horseradish peroxidase streptavidin, DAB was used for visualization and nuclei were counterstained with haematoxylin. Images were acquired using a Keyence BZ-X800 microscope (Keyence Coorporation, Osaka, Japan). Analysis of DAB stains was done using the IHC profiler plugin [25] in Fiji, including ImageJ version 1.53 (RRID: SCR_003070) [23].

Immunofluorescence

Paraffin sections of BCa organoids (6, 12 h post IR+PDT) were permeabilized as described above. Primary antibodies (Table 1) were incubated overnight at 4°C. Alexa Fluor™ 555-coupled (Goat-anti-rabbit, RRID:AB_2535849) and Alexa Fluor™ 488- coupled secondary antibodies (Goat-anti-mouse, RRID:AB_2535764) (both from Thermo Fisher Scientific, Dreieich, Germany) diluted in TBS (1 hour, room temperature), were used for indirect immunofluorescence of target proteins. Nuclei were visualized with TO-PRO-3 iodide (Cat.-No.: T3605, Thermo Fisher Scientific, Dreieich, Germany). Samples were analyzed by confocal laser scanning microscopy (LSM 800, Carl Zeiss, Jena, Germany). Fluorescence intensities (553 nm excitation/568 nm emission) of labeled targets (Casp-1, -3, -7) were quantified in CK AE-positive ROIs using Fiji (RRID: SCR_003070) [23].

Table 1: List of primary antibodies used for organoid morphology and activated pathways. Cat-No., Catalog number; Ms, mouse; Rb, rabbit; RRID, Research Resource Identification.

Antigen		Specificity	Host	Source	Cat.-No.	RRID	Dilution
panCK	DAB	Cytokeratin Pan	Ms	Sigma-Aldrich, Munich,Germany	C2931	AB_258824	1:250
Vim	DAB	Vimentin-positive cells, e.g. fibroblasts	Ms	Sigma-Aldrich, Munich,Germany	V6389	AB_609914	1:200
CD3	DAB	CD3-positive cells; T cells	Ms	ThermoFisher Scientific, Dreieich, Germany	MA5-12577	AB_10979571	1:200
CK AE	IF	Cytokeratin cocktail (AE1, AE3)	Ms	BioGenex, Fremont, CA, USA	MU071-UC	not available	1:200
Casp1	IF	Cleaved-Caspase-1 (Asp296, active)	Rb	ThermoFisher Scientific, Dreieich, Germany	PA5-99390	AB_2818323	1:200
Casp3	IF	Cleaved-Caspase-3 (Asp175, active)	Rb	Cell Signaling Technol., Frankfurt/Main, Germany	#9661	AB_2341188	1:400
Casp7	IF	Cleaved-Caspase-7 (S199, active)	Rb	Boster Biol. Technol., Pleasanton, CA, USA	A01044S199	not available	1:100

RNA extraction and qRT-PCR

For analyzing mRNA expression of pathway-specific ferroptosis markers (CHAC1, PTGS2, ACSL4, TFRC), RT-112 and T-24 organoids were incubated for additional 6, 12, 24, 48 h after IR+PDT. Total RNA was isolated with the RNeasy® Plus Micro Kit (Cat.-No.: 74034, Qiagen, Hilden, Germany) according to the manufactory manual. The lysates were homogenized by ultrasonic (5 x 15 sec) treatment. Quantitative PCR was done on a qTower3 G qPCR cycler (Analytik Jena, Jena, Germany) using Maxima SYBR-Green quantitative PCR Mastermix (Cat.-No.: K0221, Thermo Fisher Scientific, Dreieich, Germany) and custom primers (MWG-Biotech, Ebersberg, Germany) (Supplementary Table S2). The constantly expressed human glyceraldehyde-3-phosphate dehydrogenase (GAPDH) served as reference gene. Comparable efficiencies of primers used for target and housekeeping gene amplification were determined by analyzing serial cDNA dilutions.

Statistical analysis

Statistical analyses were performed using Prism 10.0.2 statistical software (RRID: SCR_002798, GraphPad Software Inc., La Jolla, CA, USA). Bar diagrams present the means + standard deviation from at least three independent experiments. Gaussian distribution of values was tested by the D´Agostino-Pearson omnibus normality test. Statistical differences were analyzed by One-way ANOVA and Mann-Whitney test. Response additivity was used as reference model [26] to evaluate synergism of treatment. Drug response values IC50 were calculated applying nonlinear regression (curve fit; inhibitor vs. response).

RESULTS

As recently described, co-culturing of BCa cells, hBF and hBSMC in 96-well ULA plates resulted in formation of bladder-like, self-organized organoids with different characteristics [22]. The study workflow is presented in Figure S3. Live cell imaging of BCa organoids demonstrated mostly completed cell separation after 48 to 72 hours of culture (Fig. S3). The treatment was conducted in accordance with dose determination experiments (Fig. S4). Preliminary experiments revealed highest cytotoxicity when using single IR dose of 9 Gy and a PDT light dose of 20 J/cm^2 (Fig. S4, A-C). Radiotherapy in combination with THPTS only or light only showed no significant effects on cell viability (Fig. S4, D).

Thus, we performed single dose IR using 9 Gy (IR 9) followed by PDT using 25 or 50 µM THPTS (PDT 25, PDT 50) and a light dose of 20 J/cm^2 on day 3 post organoid construction. After different periods of time, we analyzed cytotoxicity, tumor selectivity, cell death mode and immunogenic effects.

Concentration- and cell line-dependent cytotoxicity of IR+PDT

Cytotoxic effects of PDT and/or IR were evaluated in BCa organoids of various origin (cell lines; NMIBCa vs. MIBCa; G1-G4). Cytotoxicity was analyzed by determination of metabolic activity, organoid diameter and optical density (organoid dissociation). Concentration-dependent effects are exemplarily shown for RT-112 organoids (Fig. 1). Time-course analysis of cytotoxicity over a period of 24 to 96 h post therapy showed that the maximum differences between treated/non-treated samples were reached after 72 h (Fig. S5). The PDT monotherapy, IR monotherapy and the combination therapy showed cytotoxicity in RT-112 (after 72 h) regarding the reduction of organoid diameter. The exposure to light wíthout pre-incubation of THPTS (light only control, LOC) showed no cytotoxicity. A significant reduction in metabolic activity and organoid integrity was especially shown by the combination therapy (Fig. 1, A-C). In addition, IR+PDT treatment of RT-112 (IR 9 + PDT 50) showed synergism regarding organoid dissociation and organoid size, or additive effects in terms of metabolic

activity (Fig. 1, D). We used five different BCa cell lines to investigate cell line-dependence of effects. The therapy-related effects in different BCa organoids are presented in Figure S4. Treatment resulted in disintegration of the outer tumor cell layer in G3 BCa organoids, while morphology was hardly affected in G1/G2 organoids (Fig. S6). The various organoid types reacted very differently to the treatment. Therefore, all cytotoxicity parameters were taken into account for the analysis. Significant advantage of IR+PDT was additionally shown for RT-4, KU-19-19 and T-24 with regard to metablic activity and/or morphological changes. Interestingly, PDT in CAL-29 increased organoid viability; cytotoxicity was provoked by IR (± PDT) only (Fig. S6, C). Comparison of cell line-dependent cytotoxicity of IR+PDT vs. UTC revealed that treatment efficacy of IR+PDT seems to be in conjunction with the grading of BCa cells. In summary of all cytotoxicity parameters, G3 organoids (KU-19-19, T-24) showed the highest response to IR+PDT, while the papillary RT-4 were slightly affected by the treatment (Fig. 1, E). The response additivity analysis further demonstrated that the combinational therapy has additive or synergistic effects in all BCa organoids regarding to at least one parameter (Table S7).

Cell death mode

Cell death mechanisms provoked by IR+PDT were exemplarily analyzed in well-layered RT-112 versus loose-structured T-24 organoids (Fig. 2). Specific inhibitors against apoptosis (Z-VAD-FMK), necroptosis (necrostatin-1, GSK´872, MLKL-i) and ferroptosis (DFO, ferrostatin-1) were applied directly after PDT; cytotoxicity was analyzed via metabolic activity after 72 h. In T-24 organoids, all substances except of ferrostatin-1 led to an inhibition of cell death. In RT-112, only the iron chelator DFO resulted in a significant reduction of cytotoxicity (Fig. 2, A). Fluorescence staining against caspase-1 (pyroptosis) and caspase-3, -7 (apoptosis) was performed 6 and 12 h after IR+PDT for further evaluation of involved pathways. Increased fluorescence labeling was mainly observed in the outer tumor cell layer (Fig. 2, B). Quantification of fluorescence intensity in CK AE-positive tumor cells demonstrated significantly enhanced levels of active caspase-1 (6, 12 h), caspase-3 (6, 12 h) and caspase-7 (12 h) in RT-112 organoids. For T-24, we observed increased levels of active caspase-3 and caspase-7 after 6 h (Fig. 2, C). Since application of ferroptosis inhibitors showed contrary results in both cell lines, involvement of ferroptosis was additionally studied by qRT-PCR analysis. IR+PDT led to a significant up-regulation of all tested ferroptosis markers in RT-112 (CHAC1, PTGS2: 24 h; ACSL-4: 12, 24 h; TFRC: 6-24 h). The up-regulation in T-24 was even higher and already occurred 6 h after treatment.

Tumor-selective cytotoxicity of IR+PDT

The tumor-selective effects of the combination therapy were studied in histologically processed BCa organoids (72 h post IR+PDT), immunostained for panCK (BCa cells) and vimentin (hBF/hBSMC core). The treatment led to a significant reduction of tumor layer thickness in all tested cell lines. This effect was especially high in the G3 cell lines KU-19-19 and T-24 (50-65% reduction). In contrast, there was an increase (15-20%) in the so-called IHC OD score of vimentin in all organoid types (versus UTC), indicating a compression of the hBF/hBSMC aggregation within the organoid nucleus (Fig. 3, A, B). To analyze the effects of the combination therapy on non-malignant bladder organoids, we used the spontaneously immortalized uroepithelial cell line HBLAK. The PDT monotherapy, IR monotherapy and the combination therapy showed a significant reduction of metabolic activity in HBLAK organoids, while organoid diameter and integrity were not affected by the treatment. In addition, organoids from fibroblasts and muscle cells showed no cytotoxicity in either morphological/histological or biochemical analysis. The *standard-of-care* chemotherapeutic agent Doxorubicin, on the other hand, led to massive cell death in non-malignant organoids (HBLAK: IC_{50} = 1.820; hBF/hBSMC: IC_{50} = 0.764).

Immune cell invasion

The immunogenic effects of the treatment were investigated in a co-culture model consisting of BCa organoids and T cells. For this purpose, the organoids were treated, embedded in ECM gel and covered with a Jurkat cell supernatant. We tested the effects of PDT and IR as monotherapies and combination therapy, and we used mitoxantrone (MTX) as immunogenic reference treatment. After 3 days of co-culture, the migration of T cells into the organoid environment was analyzed (Fig. 4). Treatment of RT-112 organoids by IR+PDT resulted in significantly reduced T cell numbers in supernatants (vs. monotherapies) after co-culture, which indicated migration of Jurkats into organoid-bearing ECM. The cell numbers did not change in the untreated controls (UTC). Interestingly, the Jurkat cell counts of IR+PDT were similar to T cell numbers of MTX-treated organoids (Fig. 4, A). Immunohistochemical analysis confirmed abundance of CD3-positive T cells within the MTX- and IR+PDT-treated organoids and the surrounding ECM (Fig. 4, B). Analyses of Jurkat cell numbers in the supernatant of different G1-G4 BCa organoids demonstrated T cells migration into ECM gel containing RT-4, RT-112, T-24 and CAL-29, but not into the environment of KU-19-19 organoids.

DISCUSSION

The focal combination therapy consisiting of PDT and radiotherapy could be a promising organ-preserving alternative for treatment of bladder carcinoma. In the present study, we characterized the major cellular effects of PDT (using the photosensitizer THPTS) and ionizing radiation in vitro. Investigations on cytotoxicity, mechanisms of cell death and immunogenic effects were performed in seven different bladder organoid types (5 malignant: RT-4, RT-112, KU-19-19, T-24, CAL-29; 2 non-malignant: HBLAK, hBF/hBSMC). Treatment with PDT and/or IR resulted in reduction of metabolic activity and organoid diameter, as well as loss of morphological integrity characterized by organoid dissociation. Thereby, the various BCa organoids reacted very differently to IR+PDT. Since the high-grade organoids (G3/G4) showed the highest response rates and the papillary RT-4 showed minor response, the efficacy of IR+PDT seems to be in conjunction with the BCa cell line grading. This is in accordance with our previous studies, reporting grading-dependent effectiveness of THPTS-PDT [17] and ionizing radiation [22] in BCa cells and organoids. Response additivity analysis further revealed that the IR+PDT combination therapy has synergistic effects in all G2-G3 organoids compared to monotherapies. The advantage of a combined application of PDT (e.g. using temoporfin, palladium-bacteriopheophorbide) and radiotherapy has already been demonstrated for various tumor entities [27]. Efficacy of THPTS-PDT in combination with IR showed significant additive effects on proliferation and clonogenic survival in glioblastoma cell lines in vitro compared to monotherapies [21].

However, not all cytotoxicity parameters were equally affected in our study. For example, the treatment led to a massive destruction of the organoid structure in KU-19-19, but quantification of metabolic activity showed no differences versus untreated control. This could be explained by the complex organoid structure consisting of differently responding BCa cells in co-culture with primary bladder fibroblasts and muscle cells. Indeed, tumor-selective effects of IR+PDT were further demonstrated in histologically processed BCa organoids 72 h after treatment. We detected a reduction of the tumor cell layer in all tested cell lines. At the same time, we observed a compression of the inner hBF/hBSMC core, which indicates stabilization of 3D structure of primary cells due to better oxygen/nutrient supply following therapy-induced tumor cell death. In order to analyze the effects of PDT and IR in non-malignant 3D cultured cells, we used HBLAK organoids. In contrast to our hypothesis, HBLAK organoids were significantly affected by reduction of metabolic activity after monotherapies as well as IR+PDT. This could be explained by the genetic aberrations of HBLAKs, which are similar to that in early-stage-urothelial tumors [28]. However, PDT and/or IR had no treatment effects on primary bladder organoids consisiting of hBF and hBSMC after 72 h. This further supports the view of tumor-selective cytotoxicity provoked by IR+PDT. In comparison, *standard-of-care* chemotherapy (doxorubicin) resulted in excessive cell death (≥ 85%) in non-malignant organoids used as our „healthy bladder model“. The detected IC50 values were similar to the previously described

doxorubicin responses in BCa organoids [22]. These results illustrate the superiority of focal therapies like PDT and IR compared to conventional chemotherapies.

In addition to canonical apoptotic or necrotic cell death, both PDT and IR can induce multiple different cellular pathways (depending on the cellular context), such as pyroptosis, necroptosis and iron-dependent cell death [13,29]. Cell death mode provoked by THPTS-PDT and IR was investigated in the well-layered RT-112 versus loose-structured T-24 organoids. The induced cell death mechanisms were initially analyzed by applying specific inhibitors, and were further evaluated by analyzing pathway-specific markers. Apoptosis, necroptosis and ferroptosis were clearly identified as involved cell death pathways in T-24 organoids. In RT-112, on the other hand, there were some indications that apoptosis, ferroptosis and pyroptosis might play a role in the cytotoxicity of IR+PDT. In summary, IR+PDT led to multimodal cell death in both cell lines. Several studies showed that focal therapies, especially PDT with porphyrin photosensitizers cause tumor cell cytotoxicity by mixed cell death phenotypes [30]. For example, Turubanova et al. reported that photosens-PDT induced a mixed type of cell death with apoptotic and ferroptotic components in murine glioma cells [31]. Another approach based on PDT and methylene blue was highly effective against MDA-MB-231 breast cancer cells and led to cell death via ferroptosis and necroptosis [32].

Multimodal tumor cell death can lead to the release of immunostimulatory molecules from destroyed tumor cells mediating recruitment of immune cells [12,13]. The immunogenic effects of the treatment were investigated in a co-culture model consisting of BCa organoids and T cells. Here, a significant migration of naive T cells into the local organoid environment was demonstrated. Interestingly, the results were similar to the data obtained from treatment with the well-documented ICD-inducer MTX, which indicates the immunogenic potential of THPTS-PDT and ionizing radiation for BCa treatment. Accordingly, PDT with THPTS and IR of murine glioblastoma cells resulted in enhanced phagocytic activity of dentritic cells and cytotoxic T cell response, illustrating the immunomodulatory effect of this approach [33].

The development of a focal IR+PDT combination therapy for BCa could provide a novel effective and immunostimulatory treatment option. The bladder is easily accessible through physiological entrance via the urethra, making BCa suitable for minimally invasive treatment. In a clinical setting, THPTS could be administered topically via instillations into the urinary bladder or by intratumoral injection, and then illuminated via a transurethrally inserted light guide (e.g. glas fibre). The advantage of a local application route would be the prevention of skin sensitization by the PS. However, systemic application via intravenous administration of PS with subsequent local laser irradiation would also be conceivable. High-powered near-infrared lasers (e.g. 10-15 W) were shown to deliver light into the depth of living tissues [34], and may be suitable for this application. However, some limitations of the PDT for BCa treatment remain to be challenging: (1) the difficulty of complete and uniform illumination of the

tumor by light, (2) the difficulty of targeted PS delivery into deep regions of tumor tissue and (3) the immunosuppression within the tumor microenvironment. Indeed, imaging the tumor accumulation/penetration of THPTS is hampered by it´s chemical properties (non-fluorescent, high visible light sensitivity). The therapeutic depth of in vivo THPTS-PDT has so far been demonstrated by the visualization of dead tissue proportion in treated solid tumors [19,21]. Future research will focus on the optimization of the treatment regimen (e.g. dose adjustment, PS application techniques) of the RT+PDT combination therapy. So-called scintillating nanoparticles (NPs) that can transduce ionizing radiation into lower-energy light photons (UV/visible/near-infrared) to activate nearby PS in deep tissues are promising approaches to address the limitations. For instance, $SrAl_2O_4:Eu^{2+}$ nanoparticles were stimulated by X-ray to emit green photoluminescence (520 nm) which activated the co-loaded PS MC540 and resulted in high therapeutic depth (up to 2 cm) in a mouse xenograft model of non-small-cell lung cancer [35]. Chen et al. developed $LiGa_5O_8$:Cr- based NPs that were co-loaded with the PS 2,3-naphthalocyanine and conjugated with an anti-EGFR antibody allowing epithelial tumor targeting. IR-induced emission of near-infrared light resulted in efficient tumor suppression in an orthotopic lung carcinoma model [36]. In a recent study, You et al. encapsuled derivates of near-infrared PS (pyrene-fused (bi-) phenaziothiadiazoles) into NPs (DSPE-$mPEG_{2000}$) to efficiently induce tumor reduction in an orthotopic BCa mouse model [37]. NPs that emit light at the wavelengths corresponding to the THPTS absorption spectrum (absorption peaks: 349, 373, 516, 760 nm) could represent another potential approach. In addition, appropriate combinations with further immune cell-targeted therapies (e.g. immune checkpoint inhibitors), which break the immunosuppressive interactions between cancer and immune cells, may enhance the inherent immunogenic effects of focal therapies [38–40]. Thus, IR+PDT could enable an effective organ-sparing treatment option for bladder carcinoma.

Research data

All the data generated in this study are presented within the article or in the supplementary material. Additional information about generation or processing of data are available on request from the corresponding author.

CRediT author contribution statement

A. R.: Data curation, Investigation, Methodology, Validation. A. G.: Conceptualization, Investigation, Methodology. S. N.: Data curation, Methodology. A. W.: Data curation, Methodology. L. T.: Data curation, Methodology. J.-U. S.: Supervision. J. N.:

Conceptualization, Investigation, Writing – review and editing. M. B.-P.: Conceptualization, Data curation, Funding acquisition, Investigation, Methodology, Supervision, Visualization, Writing – original draft.

Funding

The study was supported by the German Research Foundation (DFG, grant: BE7399/1-1) and the Wissenschaftsstiftung Leipzig (Leipzig, Germany).

Conflict of interest

The authors declare no conflicts of interests.

References

[1] Ferlay J, Colombet M, Soerjomataram I, Parkin DM, Piñeros M, Znaor A, et al. Cancer statistics for the year 2020: An overview. International journal of cancer 2021.

[2] Babjuk M, Burger M, Capoun O, Cohen D, Compérat EM, Dominguez Escrig JL, et al. European Association of Urology Guidelines on Non-muscle-invasive Bladder Cancer (Ta, T1, and Carcinoma in Situ). European urology 2022;81:75–94.

[3] Witjes JA, Bruins HM, Cathomas R, Compérat EM, Cowan NC, Gakis G, et al. European Association of Urology Guidelines on Muscle-invasive and Metastatic Bladder Cancer: Summary of the 2020 Guidelines. European urology 2021;79:82–104.

[4] Antoni S, Ferlay J, Soerjomataram I, Znaor A, Jemal A, Bray F. Bladder Cancer Incidence and Mortality: A Global Overview and Recent Trends. European urology 2017;71:96–108.

[5] Rosenberg JE, Hoffman-Censits J, Powles T, van der Heijden, Michiel S, Balar AV, Necchi A, et al. Atezolizumab in patients with locally advanced and metastatic urothelial carcinoma who have progressed following treatment with platinum-based chemotherapy: a single-arm, multicentre, phase 2 trial. Lancet (London, England) 2016;387:1909–20.

[6] Bellmunt J, Wit R de, Vaughn DJ, Fradet Y, Lee J-L, Fong L, et al. Pembrolizumab as Second-Line Therapy for Advanced Urothelial Carcinoma. The New England journal of medicine 2017;376:1015–26.

[7] Manyak MJ, Ogan K. Photodynamic therapy for refractory superficial bladder cancer: long-term clinical outcomes of single treatment using intravesical diffusion medium. Journal of endourology 2003;17:633–39.

[8] Lee LS, Thong PSP, Olivo M, Chin WWL, Ramaswamy B, Kho KW, et al. Chlorin e6-polyvinylpyrrolidone mediated photodynamic therapy--A potential bladder sparing option for high risk non-muscle invasive bladder cancer. Photodiagnosis and photodynamic therapy 2010;7:213–20.

[9] Arcangeli G, Strigari L, Arcangeli S. Radical cystectomy versus organ-sparing trimodality treatment in muscle-invasive bladder cancer: A systematic review of clinical trials. Critical reviews in oncology/hematology 2015;95:387–96.

[10] Agostinis P, Berg K, Cengel KA, Foster TH, Girotti AW, Gollnick SO, et al. Photodynamic therapy of cancer: an update. CA: a cancer journal for clinicians 2011;61:250–81.

[11] Adjemian S, Oltean T, Martens S, Wiernicki B, Goossens V, Vanden Berghe T, et al. Ionizing radiation results in a mixture of cellular outcomes including mitotic catastrophe, senescence, methuosis, and iron-dependent cell death. Cell death & disease 2020;11:1003.

[12] Krysko DV, Garg AD, Kaczmarek A, Krysko O, Agostinis P, Vandenabeele P. Immunogenic cell death and DAMPs in cancer therapy. Nature reviews. Cancer 2012;12:860–75.

[13] Hänggi K, Ruffell B. Cell death, therapeutics, and the immune response in cancer. Trends in cancer 2023;9:381–96.

[14] Mroz P, Hashmi JT, Huang Y-Y, Lange N, Hamblin MR. Stimulation of anti-tumor immunity by photodynamic therapy. Expert review of clinical immunology 2011;7:75–91.

[15] Frey B, Rubner Y, Kulzer L, Werthmöller N, Weiss E-M, Fietkau R, et al. Antitumor immune responses induced by ionizing irradiation and further immune stimulation. Cancer immunology, immunotherapy : CII 2014;63:29–36.

[16] Zhu M, Yang M, Zhang J, Yin Y, Fan X, Zhang Y, et al. Immunogenic Cell Death Induction by Ionizing Radiation. Frontiers in immunology 2021;12:705361.

[17] Berndt-Paetz M, Weimann A, Sieger N, Schastak S, Riyad YM, Griebel J, et al. Tetrahydroporphyrin-tetratosylat (THPTS): A near-infrared photosensitizer for targeted and efficient photodynamic therapy (PDT) of human bladder carcinoma. An in vitro study. Photodiagnosis and photodynamic therapy 2017;18:244–51.

[18] Berndt-Paetz M, Schulze P, Stenglein PC, Weimann A, Wang Q, Horn L-C, et al. Reduction of Muscle-Invasive Tumors by Photodynamic Therapy with Tetrahydroporphyrin-Tetratosylat in an Orthotopic Rat Bladder Cancer Model. Molecular cancer therapeutics 2019;18:743–50.

[19] Schastak S, Jean B, Handzel R, Kostenich G, Hermann R, Sack U, et al. Improved pharmacokinetics, biodistribution and necrosis in vivo using a new near infra-red photosensitizer: tetrahydroporphyrin tetratosylat. Journal of photochemistry and photobiology. B, Biology 2005;78:203–13.

[20] Hubenak JR, Zhang Q, Branch CD, Kronowitz SJ. Mechanisms of injury to normal tissue after radiotherapy: a review. Plastic and reconstructive surgery 2014;133:49e-56e.

[21] Hambsch P, Istomin YP, Tzerkovsky DA, Patties I, Neuhaus J, Kortmann R-D, et al. Efficient cell death induction in human glioblastoma cells by photodynamic treatment with Tetrahydroporphyrin-Tetratosylat (THPTS) and ionizing irradiation. Oncotarget 2017;8:72411–23.

[22] Berndt-Paetz M, Han S, Weimann A, Reinhold A, Nürnberger S, Neuhaus J. Cell Line-Based Human Bladder Organoids with Bladder-like Self-Organization-A New Standardized Approach in Bladder Cancer Research. Biomedicines 2023;11.

[23] Schindelin J, Arganda-Carreras I, Frise E, Kaynig V, Longair M, Pietzsch T, et al. Fiji: an open-source platform for biological-image analysis. Nature methods 2012;9:676–82.

[24] Garg AD, More S, Rufo N, Mece O, Sassano ML, Agostinis P, et al. Trial watch: Immunogenic cell death induction by anticancer chemotherapeutics. Oncoimmunology 2017;6:e1386829.

[25] Varghese F, Bukhari AB, Malhotra R, De A. IHC Profiler: an open source plugin for the quantitative evaluation and automated scoring of immunohistochemistry images of human tissue samples. PloS one 2014;9:e96801.

[26] Duarte D, Vale N. Evaluation of synergism in drug combinations and reference models for future orientations in oncology. Current research in pharmacology and drug discovery 2022;3:100110.

[27] Viswanath D, Won Y-Y. Combining Radiotherapy (RT) and Photodynamic Therapy (PDT): Clinical Studies on Conventional RT-PDT Approaches and Novel Nanoparticle-Based RT-PDT Approaches under Preclinical Evaluation. ACS biomaterials science & engineering 2022;8:3644–58.

[28] Hoffmann MJ, Koutsogiannouli E, Skowron MA, Pinkerneil M, Niegisch G, Brandt A, et al. The New Immortalized Uroepithelial Cell Line HBLAK Contains Defined Genetic Aberrations Typical of Early Stage Urothelial Tumors. Bladder cancer (Amsterdam, Netherlands) 2016;2:449–63.

[29] Mishchenko T, Balalaeva I, Gorokhova A, Vedunova M, Krysko DV. Which cell death modality wins the contest for photodynamic therapy of cancer? Cell death & disease 2022;13:455.

[30] Alzeibak R, Mishchenko TA, Shilyagina NY, Balalaeva IV, Vedunova MV, Krysko DV. Targeting immunogenic cancer cell death by photodynamic therapy: past, present and future. Journal for immunotherapy of cancer 2021;9.

[31] Turubanova VD, Balalaeva IV, Mishchenko TA, Catanzaro E, Alzeibak R, Peskova NN, et al. Immunogenic cell death induced by a new photodynamic therapy based on photosens and photodithazine. Journal for immunotherapy of cancer 2019;7:350.

[32] Dos Santos AF, Inague A, Arini GS, Terra LF, Wailemann RAM, Pimentel AC, et al. Distinct photo-oxidation-induced cell death pathways lead to selective killing of human breast cancer cells. Cell death & disease 2020;11:1070.

[33] Rothe F, Patties I, Kortmann R-D, Glasow A. Immunomodulatory Effects by Photodynamic Treatment of Glioblastoma Cells In Vitro. Molecules (Basel, Switzerland) 2022;27.

[34] Henderson TA, Morries LD. Near-infrared photonic energy penetration: can infrared phototherapy effectively reach the human brain? Neuropsychiatric disease and treatment 2015;11:2191–208.

[35] Wang GD, Nguyen HT, Chen H, Cox PB, Wang L, Nagata K, et al. X-Ray Induced Photodynamic Therapy: A Combination of Radiotherapy and Photodynamic Therapy. Theranostics 2016;6:2295–305.

[36] Chen H, Sun X, Wang GD, Nagata K, Hao Z, Wang A, et al. LiGa5O8:Cr-based theranostic nanoparticles for imaging-guided X-ray induced photodynamic therapy of deep-seated tumors. Materials horizons 2017;4:1092–101.

[37] You C, Zhu Y, Zhu J, Xu Z, Liu Q, Wang L, et al. Strength in Numbers: A Giant NIR-II AIEgen with One-for-All Phototheranostic Features for Exceptional Orthotopic Bladder Cancer Treatment. Angewandte Chemie (International ed. in English) 2024:e202417865.

[38] Silvestrini MT, Ingham ES, Mahakian LM, Kheirolomoom A, Liu Y, Fite BZ, et al. Priming is key to effective incorporation of image-guided thermal ablation into immunotherapy protocols. JCI insight 2017;2:e90521.

[39] Arthanareeswaran V-K-A, Berndt-Paetz M, Ganzer R, Stolzenburg J-U, Ravichandran-Chandra A, Glasow A, et al. Harnessing macrophages in thermal and non-thermal ablative therapies for urologic cancers – Potential for immunotherapy. Laparoscopic, Endoscopic and Robotic Surgery 2018;1:5–11.

[40] Wang K, Wang C, Jiang H, Zhang Y, Lin W, Mo J, et al. Combination of Ablation and Immunotherapy for Hepatocellular Carcinoma: Where We Are and Where to Go. Frontiers in immunology 2021;12:792781.

FIGURE CAPTIONS

Figure 1

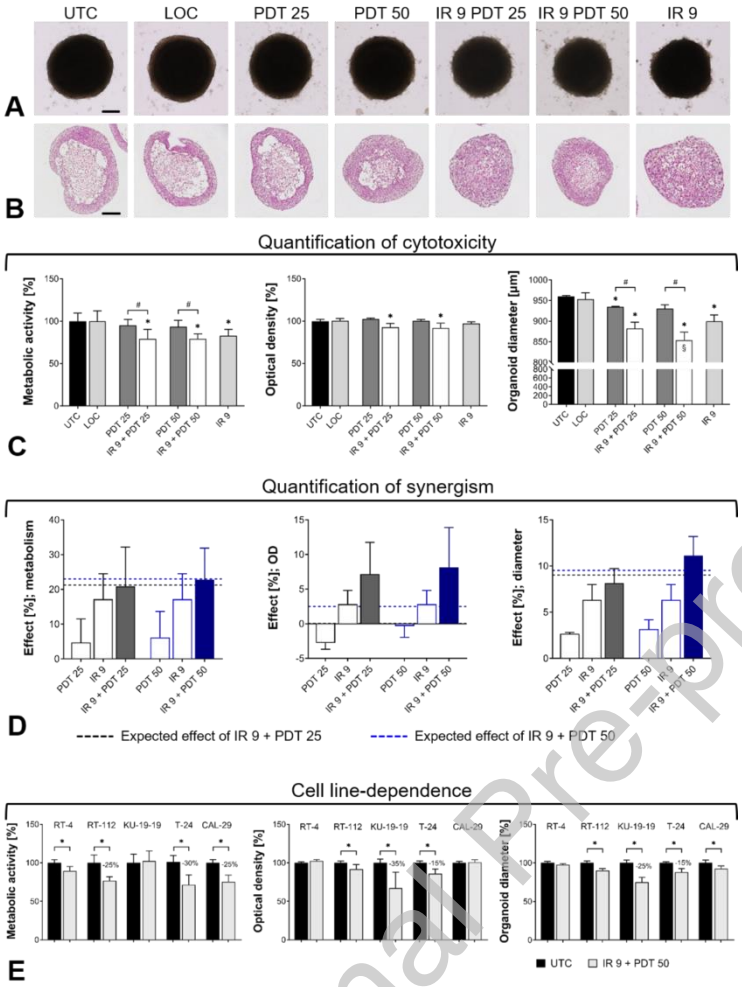

Figure 1. Cytotoxicity of PDT and/or IR in BCa organoids. (A-D) Concentration-dependent effects; exemplarily shown for RT-112 organoids. (A, B) Representative images of live microscopy (A; scale bar: 300 µm) and HE stains (B; scale bar: 200 µm) 72 h after treatment. (C) Quantification of cytotoxicity in RT-112 organoids 72 h after treatment with ionizing radiation (9 Gy) and THPTS-PDT (25, 50 µM THPTS; 20 J/cm2). Metabolic activity by CellTiter-Glo® 3D Cell Viability Assay; optical density and diameter of organoids by microscopy; * significant differences compared to untreated control (UTC); # significant differences between PDT monotherapy and combinational therapy; § significant differences between IR monotherapy and IR+PDT; * $p < 0.05$, One-way ANOVA; #,§ $p < 0.05$, Mann-Whitney test, mean + SD; n=3. (D) Response additivity analysis of cytotoxicity parameters in RT-112. Dashed lines indicate the expected effects (sum of E_{PDT} and E_{IR}; black: IR9 + PDT25; blue: IR9 + PDT50) of therapy combination. In RT-112, combinational therapy showed synergistic (optical density, diameter) or additive (metabolic activity) effects. (E) Quantification of cell line-dependent cytotoxicity in different BCa organoids 72 h after treatment with ionizing radiation (9 Gy) and THPTS-PDT (50 µM THPTS; 20 J/cm^3). Significant cytotoxic effects were observed

primarily in the higher-grade cell lines; * significant differences compared to untreated control (UTC); * $p < 0.05$, Mann-Whitney test; mean + SD; n=3.

Figure 2

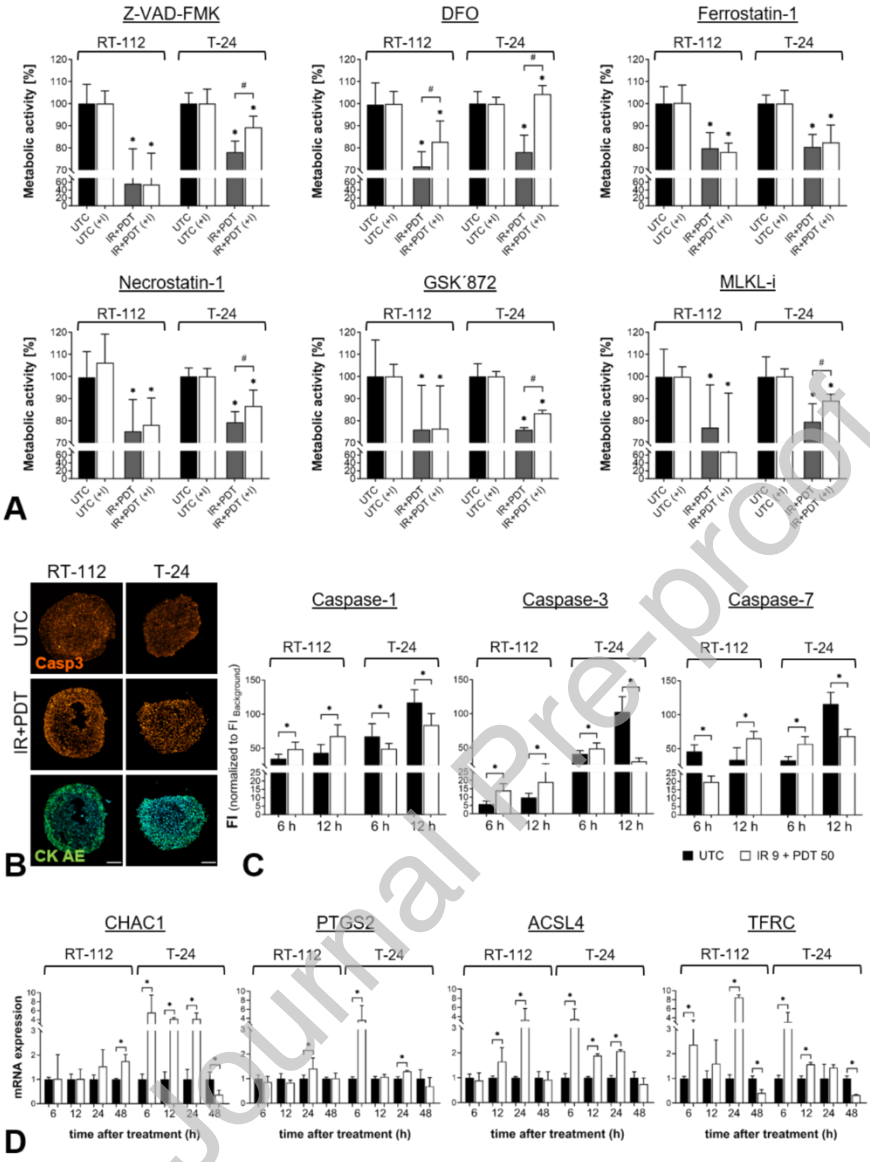

Figure 2. Cell death mode in BCa organoids treated by IR+PDT; exemplarily analyzed in RT-112 and T-24. (A) Screening on cell death pathways by applying specific inhibitors against apoptosis (Z-VAD-FMK, 25 µM), ferroptosis (ferrostatin-1, 0.5 µM; DFO, 25 µM), necroptosis (necrostatin-1, 25 µM; GSK`872, 25 µM; MLKL-i, 25 µM). Quantification of cytotoxicity 72 h after treatment with ionizing radiation (9 Gy) and THPTS-PDT (50 µM THPTS; 20 J/cm^2) by CellTiter-Glo® 3D Cell Viability Assay; * significant differences compared to untreated control (UTC); # significant differences between +/- inhibitor; * $p < 0.05$, Mann-Whitney test, mean + SD. (B, C) Analysis of activated caspases by immunofluorescence. (B) Representative immunofluorescence images of caspase-3 staining in treated vs. untreated RT-112 and T-24 organoids; scale bar: 150 µm. (C) Quantification of mean fluorescence intensity of caspases-

1, -3, -7 in CK AE-positive ROIs; 6 and 12 h after treatment. (D) Relative mRNA expression (normalized to housekeeping gene GAPDH) of ferrosptosis-associated target genes by qRT-PCR; 6, 12, 24, 48 h after treatment; * significance vs. UTC; * $p < 0.05$, Mann-Whitney test, mean + SD.

Figure 3

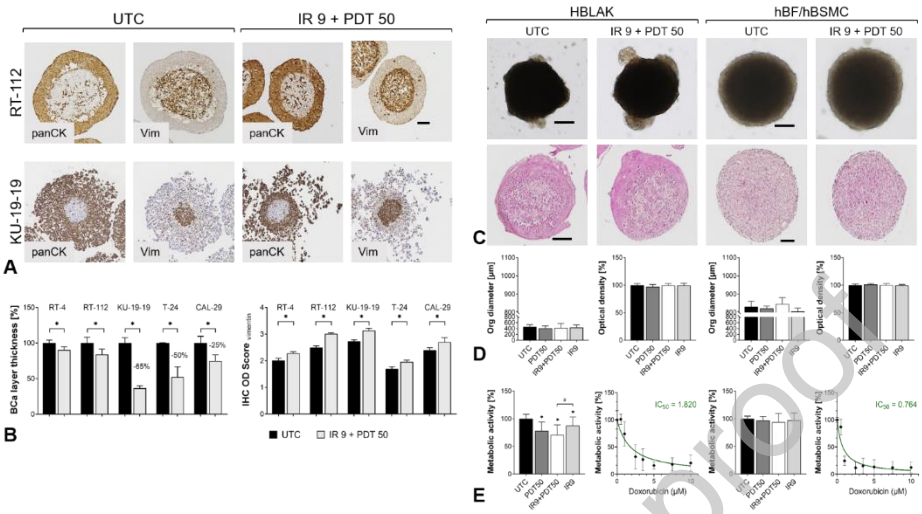

Figure 3. Effects of IR+PDT combination therapy on non-malignant cells. (A, B) Tumor-selective cytotoxicity of IR+PDT in BCa organoids. (A) Representative images of BCa organoids (treated vs. untreated controls, UTC) immunostained for panCK and vimentin (brown); exemplarily shown for well-layered RT-112 and loose-structured KU-19-19; cell nuclei (blue); scale bar: 100µm. (B) Quantification of BCa layer thickness and vimentin IHC optical density score (organoid core) in different BCa organoids 72 h after treatment with ionizing radiation (9 Gy) and THPTS-PDT (50 µM THPTS; 20 J/cm^3). Thickness of tumor cell layer decreased in all tested cell lines; while vimentin in the organoid core increased; * significant differences compared to untreated control (UTC).; $p < 0.05$, Mann-Whitney test; mean + SD; n=3. (C-E) Cytotoxicity in non-malignant organoids. (C) Representative images of live microscopy (scale bar: 150 µm) and HE stains (scale bar: 100 µm) showing HBLAK and hBF/hBSMC organoids 72 h after treatment. (D, E) Quantification of cytotoxicity in non-malignant bladder organoids 72 h after treatment with PDT and/or IR. (D) Optical density and diameter of organoids by microscopy. (E) Metabolic activity by CellTiter-Glo® 3D Cell Viability Assay; PDT and/or IR compared to dose response of doxorubicin; * significant differences compared to untreated control (UTC); # significant differences between PDT monotherapy and combinational therapy; * $p < 0.05$, One-way ANOVA; # $p < 0.05$, Mann-Whitney test, mean + SD; n=3.

Figure 4

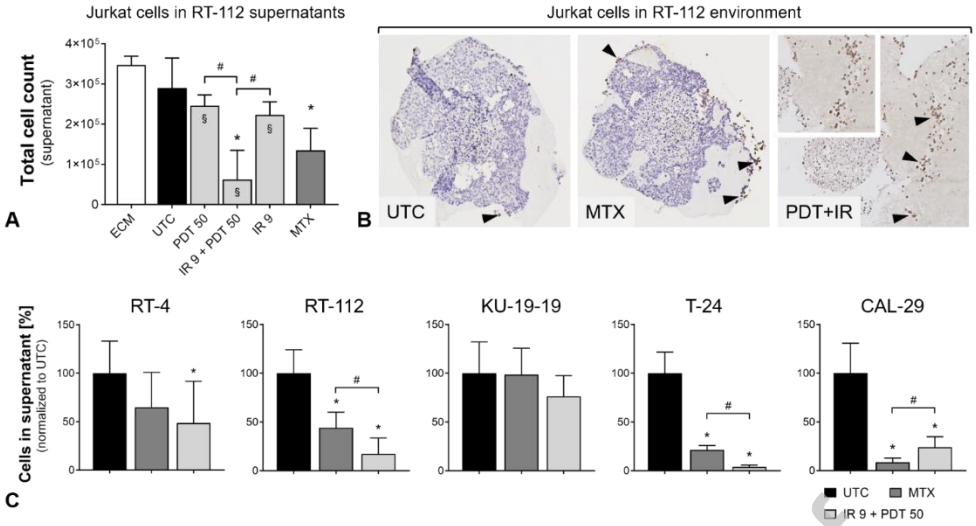

Figure 4. Invasion of human immune cells into treated BCa organoids. (A) Total numbers of Jurkat cells in the supernatant of treated and ECM-embedded RT-112 organoids (3 d after treatment). Significantly reduced T cell numbers were detected in supernatants of IR+PDT- and MTX-treated RT-112, indicating migration into the organoid environment. (B) Immunohistochemical staining revealed abundance of CD3-positive T lymphocytes (brown) in the ECM of treated RT-112 organoids. (C) Quantification of Jurkat cell numbers in the supernatant of different G1-G4 BCa organoids (RT-4, RT-112, KU-19-19, T-24, CAL-29). T cells (Jurkat) showed migration into ECM bearing RT-4, RT-112, T-24 and CAL-29 but not KU-19-19 organoids. * Significance vs. UTC; $p \leq 0.05$ (One-way ANOVA, multiple comparison test); § significance vs. MTX; # differences between IR/PDT treatment conditions; $p \leq 0.05$ (Mann-Whitney Test); mean + SD.

Conflict of Interest

The authors declare no conflicts of interest.